Sex-Stratified Aging Trajectories Reshape Cell-Type–Specific Gene Programs in Human Peripheral Immunity

Junming Chen*, Shumei Liu

Columbia University, Department of Biostatistics, New York, New York, 10032, USA

Abstract: Aging and sex are among the strongest determinants of immune phenotypes and multiple sclerosis (MS) risk, yet their joint transcriptional architecture in human blood cell subsets remains underdefined. Re-analyzing a sorted-cell bulk transcriptomic cohort (GSE137143) comprising $CD4^+$ T cells, $CD8^+$ T cells, and $CD14^+$ monocytes from adults aged 19–72 years, we quantified gene-wise age-associated expression changes (age slopes), capturing the direction and magnitude of transcriptional change across adulthood, and constructed sex-stratified weighted gene co-expression networks (WGCNA) to group genes into coordinated biological programs. Module eigengenes (MEs), which summarize the overall activity of each co-expression module, were regressed on age with cell-composition covariates; functional interpretation was supported by dual Gene Ontology enrichment strategies (over-representation analysis and preranked GSEA) to link age-associated modules to immune-relevant pathways. We further developed a sample-resolved composite visualization that orders individuals by age and annotates per-module effect sizes (β) and statistical significance, making module activity trajectories interpretable at the individual-sample level. Cross-line validation demonstrated sign concordance between gene-level age slopes and ME-level age associations, supporting that the observed aging signals reflect coherent, program-level transcriptional trajectories rather than isolated gene-level fluctuations. At the gene level, significant aging-associated genes (FDR < 0.05) were most abundant in $CD8^+$ T cells from females (329 genes) and $CD4^+$ T cells from females (72 genes), with more modest signals in males (CD8_M: 10; CD4_M: 15) and none detected in monocytes. At the module level, aging was characterized by a robust age-associated down-regulation of cell-cycle and mitotic programs in T cells—most pronounced in $CD8^+$ T cells (e.g., a representative cell-cycle module showed a strong negative age association, $P = 1.48\times10^{-8}$)—consistent with an age-related decline in proliferative capacity. In contrast, monocytes exhibited male-skewed activation of immune-receptor signaling pathways (including receptor-mediated signaling programs highlighted by GSEA) consistent with heightened innate immune activation in aging males. Female $CD4^+$ T cells showed attenuation of nuclear-division programs (e.g., nuclear-division–related pathways showed significant negative age associations in females, P = 0.022), while several female monocyte/CD4 modules were annotated by cilium/cell-projection terms, suggesting sex-dependent remodeling of cellular structure and signaling with age. Together, these results delineate sex-specific aging trajectories across immune cell types and provide reproducible analytical outputs to facilitate reuse and independent validation.

1. Introduction

Aging reshapes immunity via thymic involution, repertoire contraction, and inflammaging, while sex further modulates both immune tone and MS epidemiology [1-3]. At single-cell resolution, sex and aging jointly shape human immune-cell composition and transcription, with aged males showing higher pro-inflammatory programs and females exhibiting stronger BAFF/APRIL signaling [2]. Cell-type–resolved aging signatures can be masked in whole blood; for example, epigenetic age acceleration in MS is B-cell–biased with minimal T-cell differences, underscoring the need for subset-specific analysis [4]. Yet the joint "age × sex × cell type" transcriptional programs in sorted human blood cells remain incompletely charted, particularly with respect to coordinated, pathway-level aging effects within specific immune lineages [2,5]. Public datasets containing multiple purified subsets enable such dissection but are frequently analyzed with age/sex merely as covariates; in contrast, principled clocks and network-based approaches motivate multi-evidence frameworks that emphasize coherent biological programs reflecting shared cellular functions rather than single-gene effects [6]. Beyond composition, single-cell studies point to a ribosome-to-inflammation tradeoff as a hallmark of immune aging, providing a mechanistic prior for T-cell cycle decline and monocyte activation [7]. In disease contexts related to neuroinflammation, older MS cohorts show abnormal

*Correspondence author email: jc6342@cumc.columbia.edu

age-progressive activation/cytotoxic T-cell features [8], and CSF inhibitory/repair markers (PD-L1, Activin A) rise with age alongside disability [9], highlighting the clinical relevance of age-dependent immune remodeling.

Against this background, we reanalyzed GSE137143 to address three questions: (i) how age-associated transcriptional trajectories differ by sex within each immune cell type; (ii) which co-expression modules encode these trajectories; and (iii) which biological processes they implicate. We integrated gene-wise age coefficients, sex-stratified weighted gene co-expression networks, and dual-mode Gene Ontology enrichment, to identify coherent, sex-dependent aging programs, complemented by a sample-resolved visualization that orders individuals by age and annotates module-level effect sizes. To capture both membership- and rank-based evidence, we coupled over-representation analysis on module gene sets with GSEA on age-ranked lists, thereby constructing an atlas of sex-dependent aging modules and rendering sex-by-age effects at single-sample resolution, with direct interpretability at the pathway and individual-sample levels [2,6].

2. Methodology

2.1. Dataset and overall workflow

We re-analyzed GEO dataset **GSE137143** comprising sorted peripheral blood **CD4⁺ T**, **CD8⁺ T**, and **CD14⁺ monocyte** subsets. Each cell type was analyzed **sex-stratified** (F/M). The pipeline consisted of: phenotype harmonization → gene-level age-slope regression → sex-stratified **WGCNA** networks and module–trait association → dual **GO:BP** enrichment (**ORA** and **GSEA**) → sample-resolved composite visualization and cross-line consistency checks. All scripts and manifest files referenced below are available with the analysis [9-11].

2.2. Sample and phenotype handling

A unified sample_id was used to merge expression and traits. **Age** was auto-detected from common column aliases (e.g., age, Age, age_at_collection), requiring ≥3 finite values and non-zero variance. Sex-stratified targets were labeled as <BASE>_F and <BASE>_M[16]. When **CellPCs** were absent in traits, we merged them from 04_deconv_or_markerPC/<BASE>/markerPC_<BASE> .csv, renaming any PC*/Cell_PC* columns to CellPC* and retaining only variable PCs.

2.3. Expression inputs and preprocessing

For each (cell type × sex) stratum we used the project's processed matrices (routes 01–06). Low-abundance filtering and normalization followed the original resource; raw alignment/quantification was not altered. Gene identifiers were parsed to recover **SYMBOL** and **ENSEMBL** stems when needed for downstream mapping.

2.4. Gene-level age slopes

Within each stratum we fit per-gene linear models[8]:

$$\text{expr}_i = \alpha + \beta_{\text{age}} \cdot \text{Age}_i + \sum_k \gamma_k \, \text{CellPC}_{k,i} + \varepsilon_i$$

and reported β_{age} and Wald P. Multiple testing was controlled with **Benjamini–Hochberg FDR**. These statistics supported volcano plots and the full gene tables.

2.5. Module–age association (ME ~ Age)

For each target we regressed[17]

$$\text{ME} \sim \text{Age} + \text{CellPCs}$$

(when networks were not sex-stratified and sex01 varied, sex01 was included, but the main analysis used sex-stratified networks). We report β, standard error, P, FDR (BH), and sample size n. Correlation heatmaps were drawn for **ME × (Age + CellPCs)**.

2.6. Module gene sets and GO enrichment

For every age-associated (or near-significant with large effect) module automatically selected by 08a_standardize_and_align.R (default: **top 2 modules per target** by P then |β|), we wrote module members and mapped them to **ENTREZ** and **SYMBOL** using **clusterProfiler/OrgDb** [2,3].

- **Over-representation analysis (ORA)**: enrichGO(ont="BP", keyType="ENTREZID", OrgDb=org.Hs.eg.db), BH adjusted (**p.adj < 0.05**, **q < 0.2**).
- **GSEA**: preranked by a kME-like score (gene–ME Pearson correlation; direction aligned to ME~Age β); gseGO(ont="BP", minGS=10, maxGS=5000). We display dotplots and leading-edge running-score plots. For speed-robustness we relied on clusterProfiler's GSEA implementation (conceptually equivalent to Subramanian et al.) [4], with parameters chosen to balance sensitivity and term breadth[12-15].

2.7. Sample-resolved composite visualization

09_cluster_host_composite. R orders samples by **Age**, visualizes per-sample **ME z-scores** (color; point size ∝ |z|), and annotates the per-panel regression β and P (ME ~ Age + CellPCs). This creates a compact, traceable view linking effect direction, significance, and age ordering at the individual level.

2.8. Sex-difference pairing and cross-line consistency

Female and male modules sharing the same ME label within a base cell type were paired to compute **Δ = β_F − β_M** and visualized as a one-column heatmap/bar plot[18]. We further compared ME-level β signs to the mean gene-level β_{age} within the same module (independent

processing route) to assess **sign concordance** across methods.

2.9. Statistics and software

Unless stated otherwise, tests were **two-sided**; BH-FDR controlled multiplicity for module testing (within target) and for GO terms[19]. We report β, P, FDR, 95% CIs where appropriate, and sample sizes. Analyses ran in **R (≥4.x)** with the following key packages: **WGCNA** [1], **clusterProfiler** [2], **org.Hs.eg.db** [3], **enrichplot**, **igraph** [5], **ggplot2**, **pheatmap**, and **officer** (for PPT assembly). Script names and roles[15]:

- 07d_MEs_traits_age_only.R — traits completion, ME×trait heatmaps, ME~Age regressions
- 08a_standardize_and_align.R — standardized exports, ID mapping, ORA/GSEA, F–M Δ pairing
- 08b_pretty_networks.R — TOM/adjacency subgraphs and aesthetic plotting
- 08a_patch_me_stats.R / _FIXED.R — harmonized ME~Age statistics and master tables

2.10. Sex-difference pairing and cross-line consistency

Raw data are available at **GEO: GSE137143**. All scripts, parameters, and standardized outputs (e.g., _ME_master.csv, _ME_master_pairs_delta.csv, _figure_inventory.csv, and per-module module_genes_mapped_ENTREZ.csv) will be released upon acceptance; read-only access can be provided during peer review.

3. Result

3.1. Cohort and networks

Table 1. Cohort characteristics by cell type and sex

cell_type	sex	n_samples	age_mean	age_sd	age_min	age_max
CD14	F	77	36.79	10.1	21	72
CD14	M	43	36.91	10.55	19	66
CD4	F	76	37	10	21	72
CD4	M	42	36.95	10.67	19	66
CD8	F	76	37	10	21	72
CD8	M	43	36.79	10.54	19	66

We analyzed 120 CD14⁺ (77F/43M), 118 CD4⁺ (76F/42M), and 119 CD8⁺ (76F/43M) samples (mean age≈37y, SD≈10y; range 19–72y per cell type). The cohort characteristics by cell type and sex are summarized in Table 1, and An overview of the cohort structure and gene-level aging signals is shown in Figure 1. Signed WGCNA (softPower=8) yielded: CD14: 8 modules (sizes: turquoise 1789, blue 1410, brown 1291, yellow 886, green 115, red 78, black 60; grey 4371). CD4: 9 modules (turquoise 1338, blue 1177, brown 657, yellow 123, green 107, red 89, black 66, pink 55; grey 6388). CD8: 12 modules (turquoise 1957, blue 1194, brown 976, yellow 702, green 246, red 240, black 142, pink 127, magenta 66, purple 65, greenyellow 33; grey 4252). The WGCNA parameters and module inventories are summarized in Table 3. These settings were identical between female and male strata to facilitate comparison.

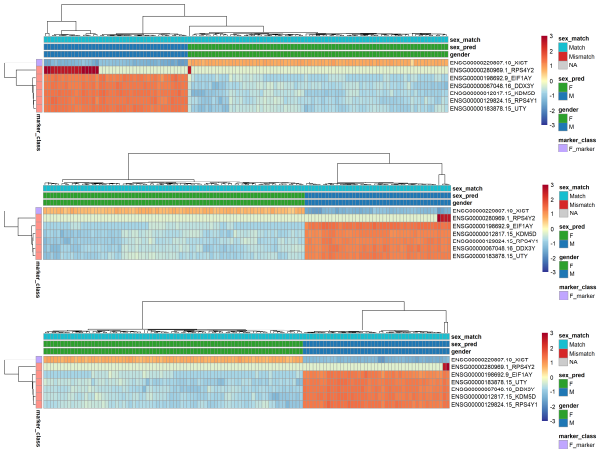

Figure 1. Cohort overview and gene-level aging signals.

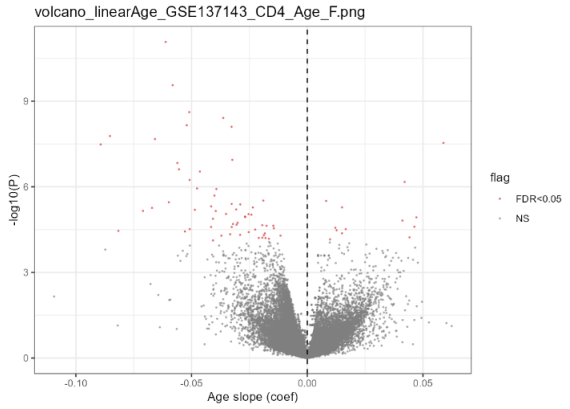

(a)

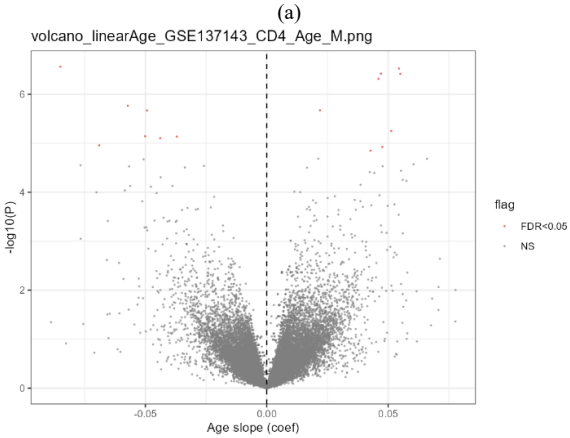

(b)

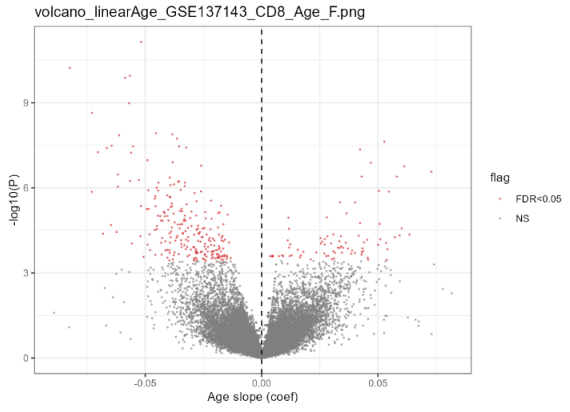

(c)

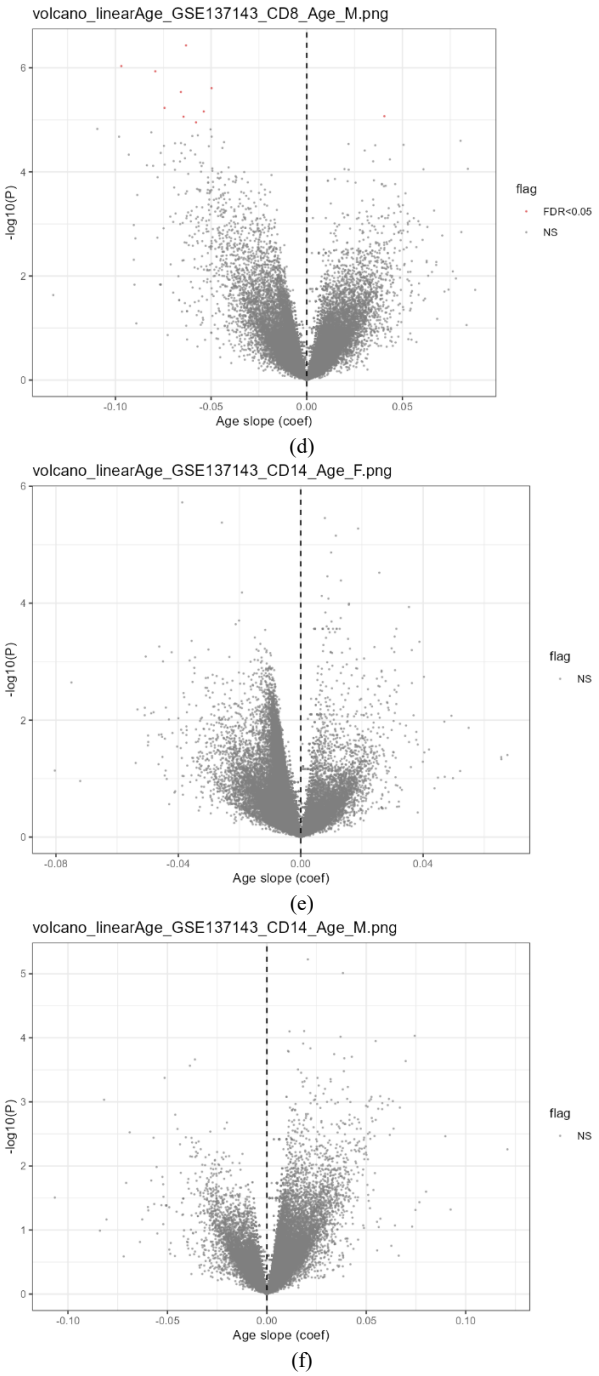

Figure 2. (a). Per-gene age-associated expression volcano plot in female CD4⁺ T cells. (b). Per-gene age-associated expression volcano plot in male CD4⁺ T cells. (c). Per-gene age-associated expression volcano plot in female CD8⁺ T cells. (d). Per-gene age-associated expression volcano plot in male CD8⁺ T cells. (e). Per-gene age-associated expression volcano plot in female CD14⁺ monocytes. (f). Per-gene age-associated expression volcano plot in male CD14⁺ monocytes.

3.2. Gene-level aging signals are cell-type and sex dependent

Per-gene regressions (β_age) revealed strong signals in CD8_F (329 genes, FDR<0.05) and CD4_F (72), with smaller sets in CD8_M (10) and CD4_M (15), and CD14_F/M (0). These cell-type- and sex-stratified gene-level aging signals are visualized in Figure 2, and a summary of the gene-level age association results is provided in Table 2. Only one gene survived in the CD8 F–M difference analysis (FDR<0.05). This motivated a move from dispersed gene-wise signals to coherent modules.

Table 2 Gene-level age associations summary (a–f)

target	contrast	n_genes	n_sig_FDR05	n_samples
CD14_F	Age_F	44328	0	77
CD14_FminusM	Diff_FminusM	44328	0	120
CD14_M	Age_M	44328	0	43
CD4_F	Age_F	44328	72	76
CD4_FminusM	Diff_FminusM	44328	0	118
CD4_M	Age_M	44328	15	42
CD8_F	Age_F	44328	329	76
CD8_FminusM	Diff_FminusM	44328	1	119
CD8_M	Age_M	44328	10	43

Table 3 WGCNA parameters and module inventories (a–f)

target	softPower	networkType	corType	minModuleSize	deepSplit	mergeCutHeight	nModules
GSE137143_ALL_F	8	signed	pearson	30	2	0.25	11
GSE137143_ALL_M	8	signed	pearson	30	2	0.25	11
GSE137143_CD14_F	8	signed	pearson	30	2	0.25	8
GSE137143_CD14_M	8	signed	pearson	30	2	0.25	8
GSE137143_CD4_F	8	signed	pearson	30	2	0.25	9
GSE137143_CD4_M	8	signed	pearson	30	2	0.25	9
GSE137143_CD8_F	8	signed	pearson	30	2	0.25	12
GSE137143_CD8_M	8	signed	pearson	30	2	0.25	12

3.3. Module-level age associations highlight T-cell cell-cycle decline and monocyte activation

Regressing ME~Age (per stratum) identified sentinel modules, the module-level associations with age and cell-composition covariates are shown in Figure 3.:

CD8 T cells

- ME6_red: $\beta=-4.45\times10^{-3}$, $P=1.48\times10^{-8}$, $FDR=1.77\times10^{-7}$ (n=119).
- ME8_pink: $\beta=-1.82\times10^{-3}$, P=0.0285 (FDR=0.0856).
- ME10_purple: $\beta=+3.83\times10^{-3}$, $P=1.69\times10^{-6}$, $FDR=1.02\times10^{-5}$.

Enrichment for "chromosome segregation" (ORA $q=2.42\times10^{-30}$) and GSEA "mitotic cell cycle" (NES=−2.70, $q=2.57\times10^{-5}$) marks a declining proliferative program with age, particularly in the male composite panels. The ORA and GSEA results for male

CD8⁺ T cells are shown in Figure 7. The GSEA results for female CD8⁺ T cells are shown in Figure 6. This pattern is consistent with single-cell evidence that translational capacity declines while inflammatory tone rises with age [7].

CD4 T cells

- ME6_red shows nuclear-division biology (ORA "nuclear division" $q=1.73\times10^{-26}$). The corresponding ORA and GSEA results for female CD4⁺ T cells are shown in Figure 4. In the composite regression using host terms, CD4_F_ME6 had $\beta=-0.049$, $P=0.022$ ($n=40$ subsampled), consistent with a female-biased attenuation of cycle programs.
- ME2_blue (CD4_M) is immune-receptor–linked (ORA "immune response-regulating receptor signaling" $q=2.09\times10^{-22}$; GSEA "defense response" NES=+2.26, $q=1.39\times10^{-7}$). The corresponding enrichment results for male CD4⁺ T cells are shown in Figure 5.

CD14 monocytes

- CD14_M ME1_turquoise: GSEA "T cell receptor signaling" NES=+3.20, $q=7.17\times10^{-9}$; ORA "antigen receptor–mediated signaling" $q=4.95\times10^{-18}$—activation tone rises with age, especially in males. The corresponding ORA and GSEA results for male CD14⁺ monocytes are shown in Figure 9. This aligns with population-level increases of monocyte fractions and inflammatory programs with aging [2,5].
- CD14_F showed cilium/cell-projection terms (e.g., "cilium movement" q=0.0038), suggesting structural remodeling rather than strong monotone age trends. The enrichment results for female CD14⁺ monocytes are shown in Figure 8.

Notably, in the master F–M paired table the Δβ for ME vs. age is ≈0 for several bases, reflecting that module definitions and ME regressions were constrained to be comparable across sexes; nevertheless, the GO content and the sample-resolved β estimates (route 09) reveal sex-skewed biology (e.g., CD8_M cell-cycle decline; CD14_M immune activation).

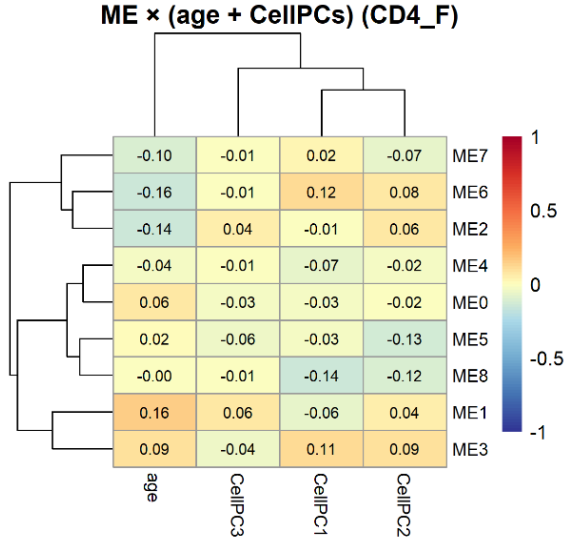

(a)

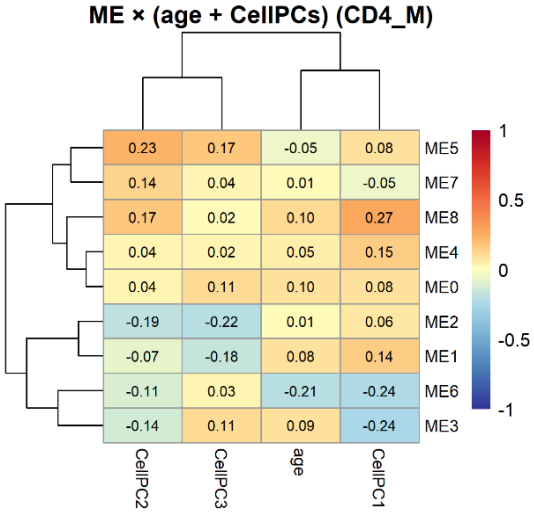

(b)

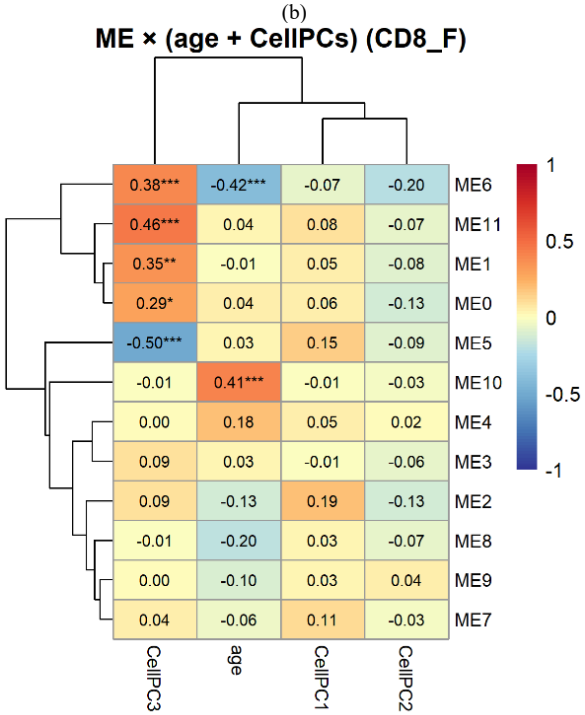

(c)

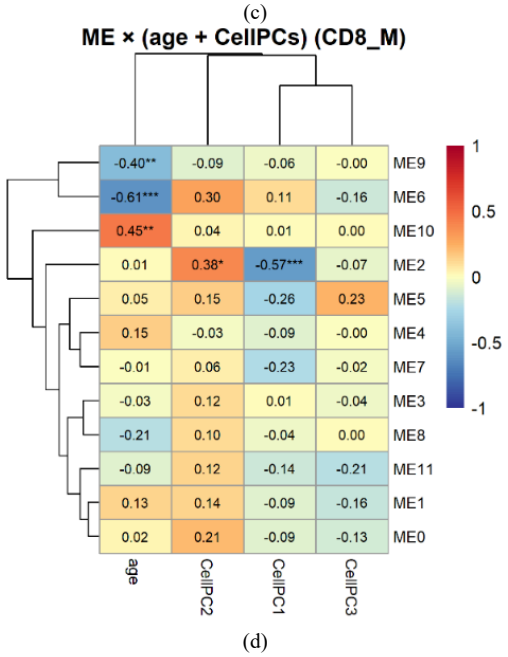

(d)

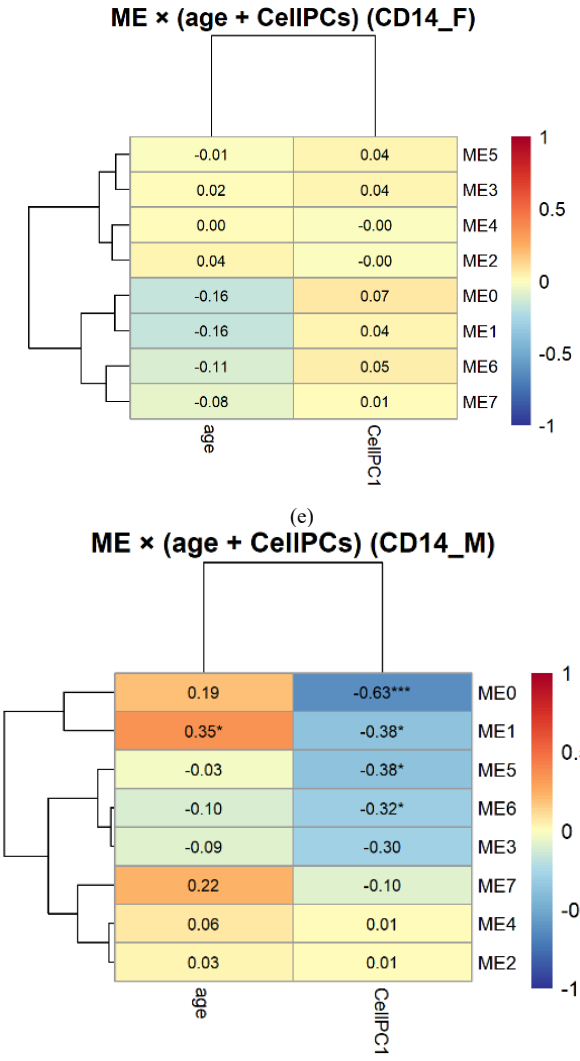

Figure 3. (a). Module-level associations with age and cell composition in female CD4⁺ T cells. (b). Module-level associations with age and cell composition in male CD4⁺ T cells. (c). Module-level associations with age and cell composition in female CD8⁺ T cells. (d). Module-level associations with age and cell composition in male CD8⁺ T cells. (e). Module-level associations with age and cell composition in female CD14⁺ monocytes. (f). Module-level associations with age and cell composition in male CD14⁺ monocytes.

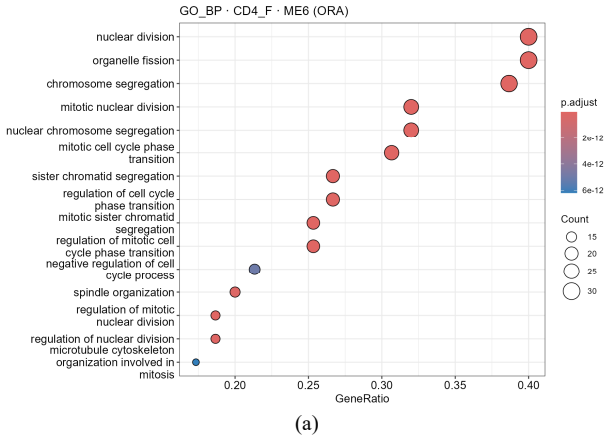

(a)

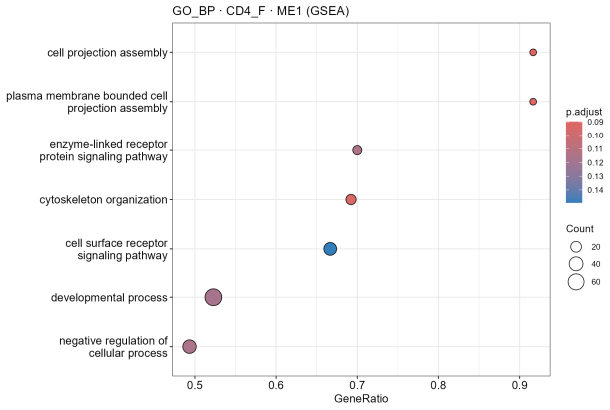

(b)

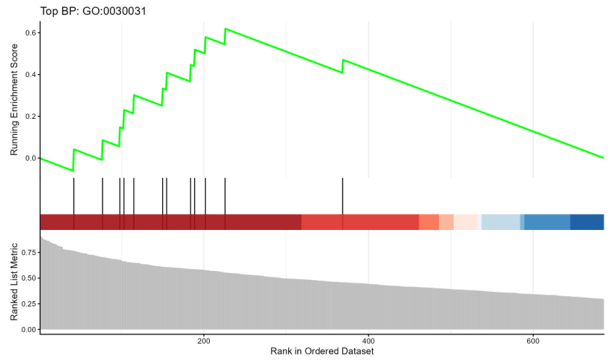

(c)

Figure 4. (a). Gene Ontology biological process enrichment of an age-associated module in female CD4⁺ T cells (ORA). (b). Gene Ontology biological process enrichment of age-associated modules in female CD4⁺ T cells (GSEA). (c). GSEA enrichment plot of a representative Gene Ontology biological process in female CD4⁺ T cells.

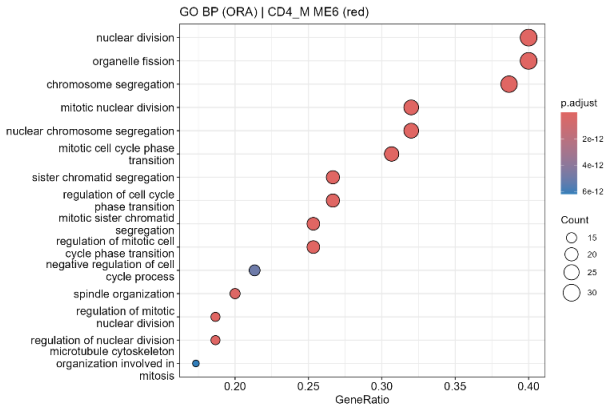

(a)

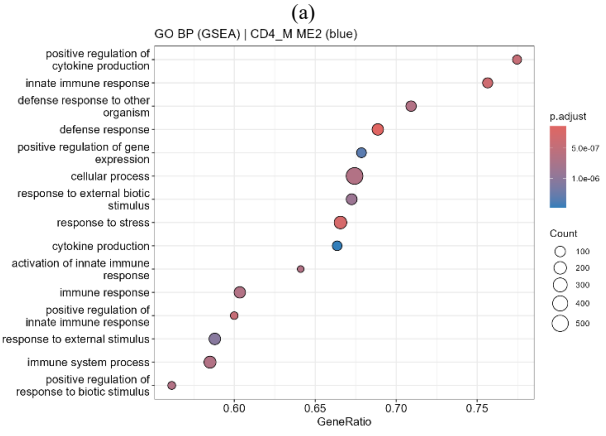

(b)

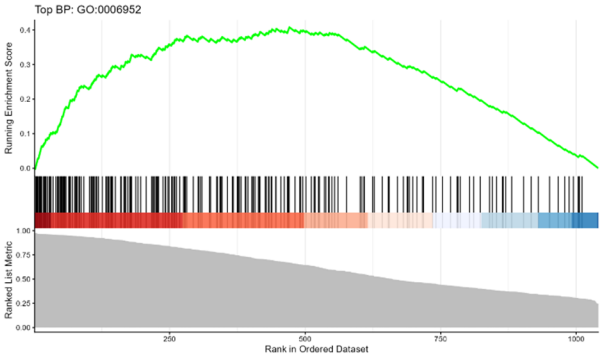

(c)

Figure 5. (a). Gene Ontology biological process enrichment of an age-associated module in male CD4⁺ T cells (ORA). (b). Gene Ontology biological process enrichment of age-associated modules in male CD4⁺ T cells (GSEA). (c). GSEA enrichment plot of a representative Gene Ontology biological process in male CD4⁺ T cells.

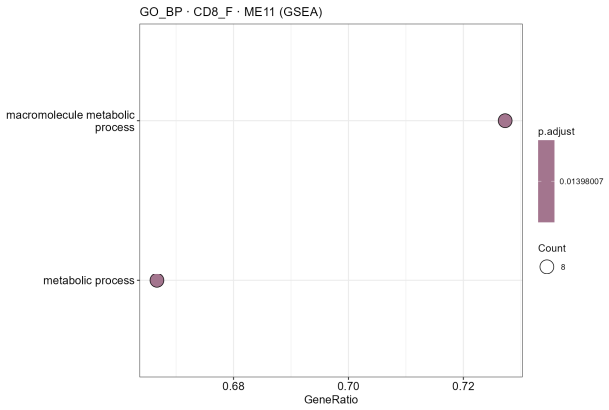

(a)

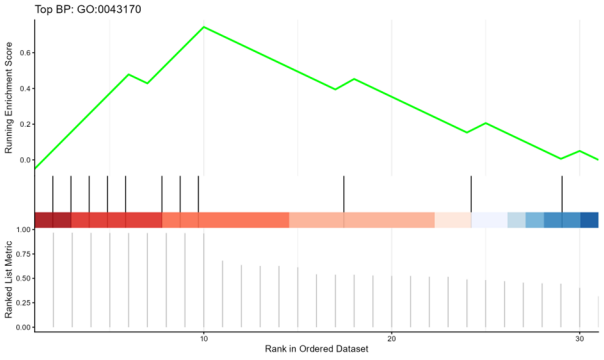

(b)

Figure 6. (a). Gene Ontology biological process enrichment of age-associated modules in female CD8⁺ T cells (GSEA). (b). GSEA enrichment plot of a representative Gene Ontology biological process in female CD8⁺ T cells.

3.4. Composite, sample-resolved panels make trajectories legible

Our "host-cluster composite" panels order samples by age, plot ME z-scores (color, |z| as point size), and print β and P per (host term × module × stratum). Examples:

Male CD8, host "regulation of primary metabolic process" (from ME6_red): β=−0.076, P=7.0×10⁻⁶ (n=40), a steep decline across the age axis.

Male CD8, host "spindle assembly" (ME8_pink): β=−0.034, P=0.138.

Female CD4, host "regulation of chromosome separation" (ME6_red): β=−0.049, P=0.022.

This format tightly connects direction, significance, and age ordering at the sample level.

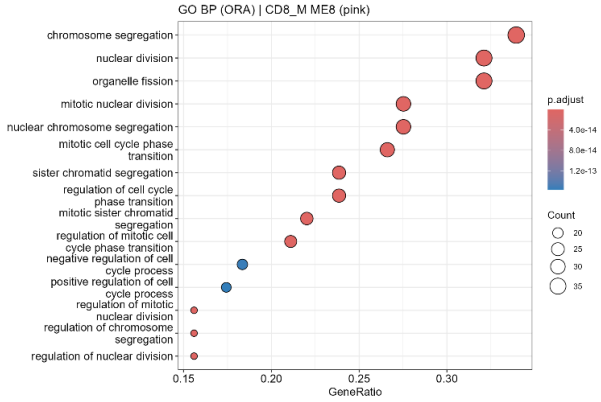

(a)

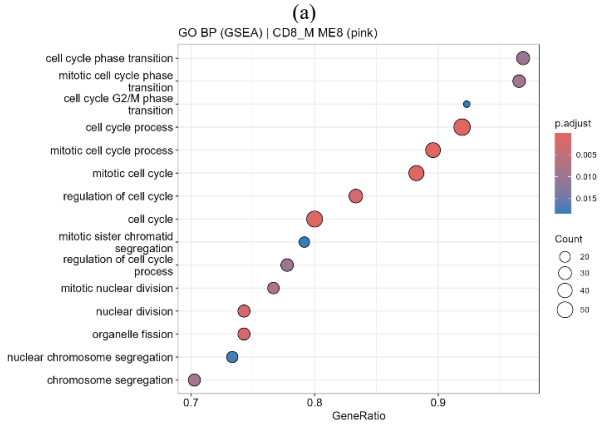

(b)

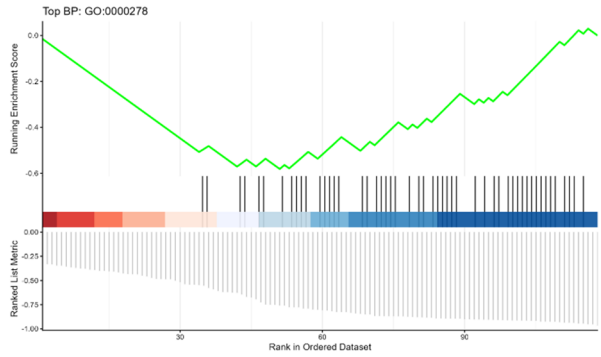

(c)

Figure 7. (a). Gene Ontology biological process enrichment of an age-associated module in male CD8⁺ T cells (ORA). (b). Gene Ontology biological process enrichment of age-associated modules in male CD8⁺ T cells (GSEA). (c). GSEA enrichment plot of a representative Gene Ontology biological process in male CD8⁺ T cells.

3.5. Dual GO corroboration across ends of the rank spectrum

For each module we paired ORA on membership genes with GSEA on age-ranked lists. Cycle terms (mitosis/chromosome segregation) recur in CD8/CD4 modules with strong FDR control; receptor/defense

signaling dominates CD4_M and CD14_M; cilium/cell-projection terms appear in female subsets. Leading-edge annotations (e.g., tags/list/signal for CD8_M) indicate broad gene set engagement. Given that no single measurement captures aging complexity, this dual-evidence design improves robustness [6,12,13].

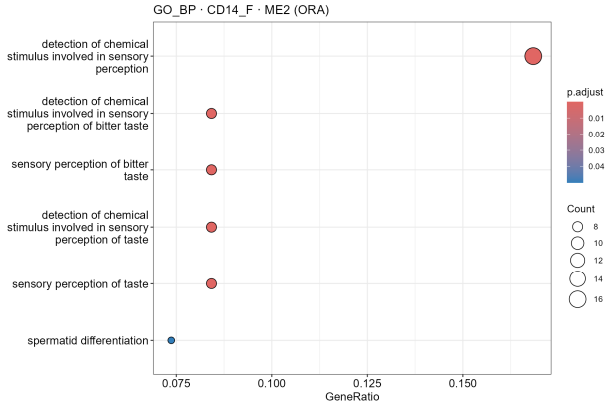

(a)

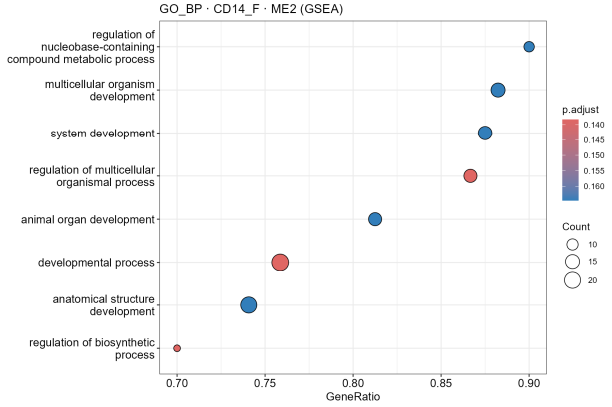

(b)

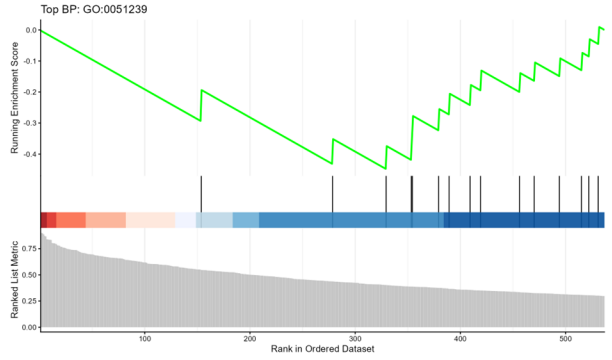

(c)

Figure 8. (a). Gene Ontology biological process enrichment of an age-associated module in female CD14⁺ monocytes (ORA). (b). Gene Ontology biological process enrichment of age-associated modules in female CD14⁺ monocytes (GSEA). (c). GSEA enrichment plot of a representative Gene Ontology biological process in female CD14⁺ monocytes.

3.6. Cross-line validation

Comparing ME β (routes 07–09) with mean gene-level β (route 06) across sentinel modules showed sign concordance in all tested cases (e.g., CD8 cell-cycle modules negative in both routes). The sample-resolved composite panels and cross-route concordance analysis are summarized in Figure 10.

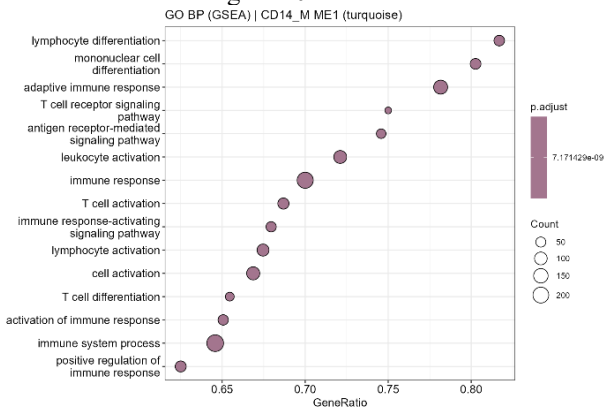

(a)

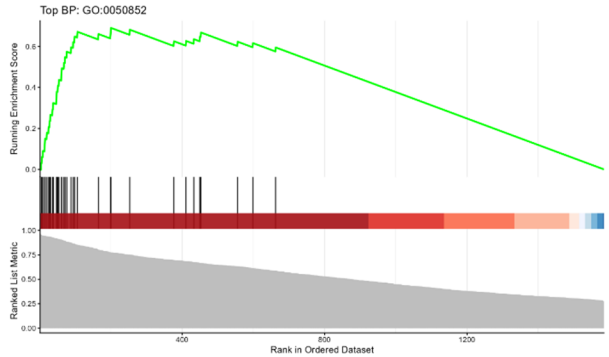

(b)

Figure 9 (a). Gene Ontology biological process enrichment of age-associated modules in male CD14⁺ monocytes (GSEA). (b). GSEA enrichment plot of a representative Gene Ontology biological process in male CD14⁺ monocytes.

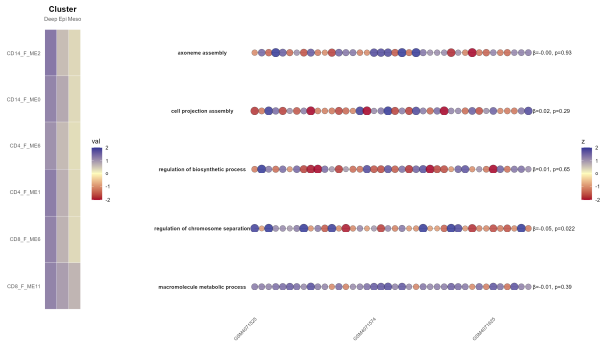

(a)

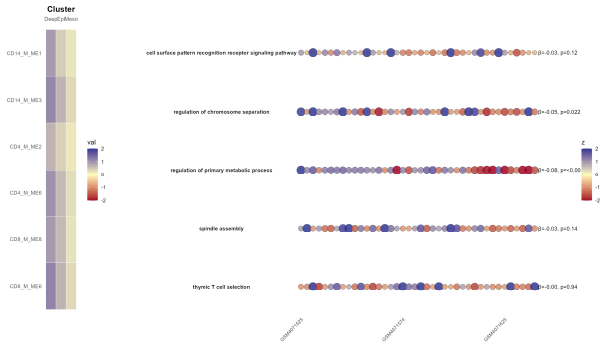

(b)

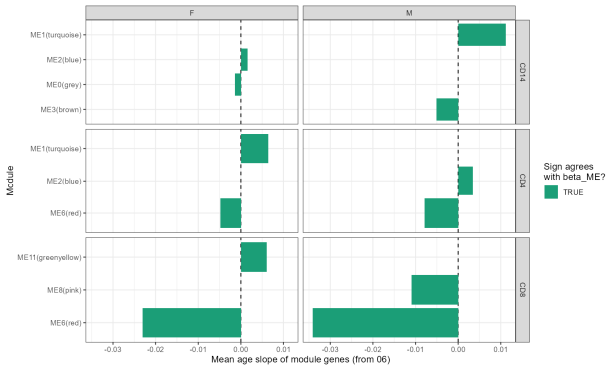

(c)

Figure 10. (a). Sample-resolved host–cluster composite panel in females highlighting axoneme/cell-projection and chromosome-separation programs. (b). Sample-resolved host–cluster composite panel in males highlighting pattern-recognition receptor signaling, metabolic regulation, and mitotic programs. (c). Cross-route concordance between module-level and gene-level age effects.

4. Discussion

Our analysis delineates a sex-stratified aging atlas across human CD4$^+$, CD8$^+$, and CD14$^+$ subsets, revealing distinct, cell-type–specific biological trajectories of immune aging. The most consistent pattern is a decline of cell-cycle and mitotic programs in T cells—largest in CD8 and especially evident in males—paralleling an age-related reduction in proliferative capacity, consistent with prior evidence that aging T cells shift from homeostatic proliferation toward more differentiated or effector-biased states, with a concurrent rise of receptor and defense signaling in male monocytes, suggesting that innate immune compartments may disproportionately contribute to age-associated inflammatory tone in males. Female-specific signals include attenuation of nuclear-division programs in CD4 T cells and cilium and cell-projection remodeling in monocytes, potentially reflecting sex-dependent changes in cellular structure, motility, or immune sensing rather than canonical ciliary function, suggesting sex-dependent modes of immune aging beyond proliferative decline. Together, these axes refine the concept of inflammaging by exposing cell-type– and sex-resolved modules and their biological labels, thereby linking age-associated transcriptional change to specific immune processes across sexes [1–3,7–9]. Importantly, the cross-level agreement between gene-wise age slopes and module-level age associations strengthens confidence that these patterns represent reproducible, cell-type–specific aging programs rather than analysis-dependent artifacts.

Limitations: This study represents a secondary analysis without wet-lab validation; clinical covariates beyond composition PCs were unavailable; and $\Delta\beta$ at the ME level can be conservative when module definitions are harmonized. Some cilium-related enrichments should be orthogonally checked.

Implications and next steps: Test age × sex × disease interactions within this cohort; replicate findings in independent datasets (sorted or high-quality deconvolution); and pursue targeted validation (e.g., Ki-67, phospho-RB, and mitotic spindle markers in T cells; TCR and innate signaling readouts in monocytes). These steps would raise evidentiary strength and mechanistic confidence for higher-impact venues.

5. Conclusion

In conclusion, this study provides a sex-stratified and cell-type–resolved view of immune aging in human peripheral blood. By integrating gene-level age slopes, WGCNA-based co-expression modules, dual Gene Ontology enrichment strategies, and sample-resolved visualization, we identified coherent aging-associated transcriptional programs across CD4$^+$ T cells, CD8$^+$ T cells, and CD14$^+$ monocytes. The most prominent aging signature was the down-regulation of cell-cycle and mitotic programs in T cells, particularly in CD8$^+$ T cells, suggesting an age-related decline in proliferative capacity. In contrast, monocytes, especially in males, showed enrichment of immune-receptor and inflammatory signaling programs, supporting a sex-skewed contribution of innate immune activation to aging-associated immune remodeling. Female-specific patterns, including attenuation of nuclear-division programs in CD4$^+$ T cells and cilium/cell-projection-related enrichment in monocytes, further indicate that immune aging proceeds through distinct biological routes across sex and cell type. Overall, these findings highlight the importance of considering age, sex, and immune-cell identity jointly when characterizing human immune aging and provide a reproducible analytical framework for future validation in independent cohorts and disease-relevant settings.

Acknowledgements

JunMing Chen and Shumei Liu contributed equally to this work and should be considered co-first authors.

References

1. Dema M, Eixarch H, Villar LM, Montalban X, Espejo C. (2021) Immunosenescence in multiple sclerosis: The identification of new therapeutic targets. Autoimmun Rev. 2021; 20: 102893. doi: 10.1016/j.autrev.2021.102893.
2. Huang Z, Chen B, Liu X, et al. (2021) Effects of sex and aging on the immune cell landscape as assessed by single-cell transcriptomic analysis. Proc Natl Acad Sci U S A. 2021;118(33):e2023216118
3. Amoriello R, Mariottini A, Ballerini C. (2021) Immunosenescence and autoimmunity: Exploiting the T-cell receptor repertoire to investigate the impact of aging on multiple sclerosis. Front Immunol. 2021; 12: 799380. doi:10.3389/fimmu.2021.799380
4. Maltby JV, Campagna MP, Horn H, et al. (2023) Evaluation of cell-specific epigenetic age acceleration in people with multiple sclerosis.

Neurology. 2023; 101: e679–e689. doi: 10.1212/WNL.0000000000207489

5. Luo OJ, Lei W, Zhu G, et al. (2022) Multidimensional single-cell analysis of human peripheral blood reveals characteristic features of the immune system landscape in aging and frailty. Nat Aging. 2022; 2: 348–364. doi:10.1038/s43587-022-00198-9
6. Li S, Wang K, Wu J, Zhu Y. (2025) The immunosenescence clock: A new method for evaluating biological age and predicting mortality risk. Ageing Res Rev. 2025;104:102653. doi:10.1016/j.arr.2024.102653
7. Zhu H, Chen J, Liu K, et al. (2023) Human PBMC scRNA-seq–based aging clocks reveal ribosome to inflammation balance as a single-cell aging hallmark and super longevity. Sci Adv. 2023;9:eabq7599. doi:10.1126/sciadv.abq7599
8. Zuroff L, Rezk A, Shinoda K, et al. (2022) Immune aging in multiple sclerosis is characterized by abnormal CD4 T cell activation and increased frequencies of cytotoxic CD4 T cells with advancing age. EBioMedicine. 2022;82:104179. doi:10.1016/j.ebiom.2022.104179
9. Picón C, Tejeda-Velarde A, Fernández-Velasco JI, et al. (2021) Identification of the immunological changes appearing in the CSF during the early immunosenescence process occurring in multiple sclerosis. Front Immunol. 2021;12:685139. doi:10.3389/fimmu.2021.685139
10. Gavrish A, Chistyakov P, Sergeeva M, et al. (2021) ARGEOS: A Web Tool for Systematic Search and Structured Retrieval of Transcriptomic Studies from GEO and ArrayExpress. Biology (Basel). 2021;10(10):1026. doi:10.3390/biology10101026
11. Hampton TH, Stanton BA, et al. (2022) CF-Seq: an accessible web application for rapid re-analysis of cystic fibrosis pathogen RNA sequencing studies. Sci Data. 2022;9(1):343. doi:10.1038/s41597-022-01431-1
12. Huang Z, Han Z, Wang T, et al. (2021) TSUNAMI: Translational Bioinformatics Tool Suite for Network Analysis and Mining. Genomics Proteomics Bioinformatics. 2021;19(6):1023-1031. doi:10.1016/j.gpb.2019.05.006
13. Callegaro G, Kunnen SJ, Trairatphisan P, et al. (2021) The human hepatocyte TXG-MAPr: gene co-expression network modules to support mechanism-based risk assessment. Arch Toxicol. 2021;95(12):3745-3775. doi:10.1007/s00204-021-03141-w
14. García-Nieto E, Rodriguez-Duque JC, Rivas-Rivas C, et al. (2024) Clinical and molecular characterization of steatotic liver disease in the setting of immune-mediated inflammatory diseases. JHEP Rep. 2024;6:101167. doi:10.1016/j.jhepr.2024.101167
15. Alkhatabi HA, Pushparaj PN. (2024) Untangling the complex mechanisms associated with Alzheimer's disease in elderly patients using high-throughput RNA sequencing data and next-generation knowledge discovery methods. Heliyon. 2024;10:e41266. doi:10.1016/j.heliyon.2024.e41266
16. Huang Z, Chen B, Liu X, et al. (2021) Effects of sex and aging on the immune cell landscape as assessed by single-cell transcriptomic analysis. Proc Natl Acad Sci U S A. 2021;118(33):e2023216118. doi:10.1073/pnas.2023216118
17. Callegaro G, Kunnen SJ, Trairatphisan P, et al. (2021) The human hepatocyte TXG-MAPr: gene co-expression network modules to support mechanism-based risk assessment. Arch Toxicol. 2021;95(12):3745–3775. doi:10.1007/s00204-021-03141-w
18. Langfelder P, Horvath S. (2008) Weighted correlation network analysis (WGCNA): an R package for weighted correlation network analysis. BMC Bioinformatics. 2008;9:559. doi:10.1186/1471-2105-9-559
19. Benjamini Y, Hochberg Y. (1995) Controlling the false discovery rate: a practical and powerful approach to multiple testing. J R Stat Soc Series B Stat Methodol. 1995;57(1):289-300